Cell Exclusion in Couette Flow: evaluation through flow visualisation and mechanical forces

Author

Leslie, LJ, Marshall, LJ, Devitt, A, Hilton, A, Tansley, GD

Published

2013

Journal Title

Artificial Organs

DOI

10.1111/j.1525-1594.2012.01561.x

Cell Exclusion in Couette Flow: Evaluation through flow visualisation and mechanical forces

Laura J Leslie[1], Lindsay J Marshall[2], Andrew Devitt[3], Andy Hilton[4] and Geoff D Tansley[5]

[1]School of Engineering and Applied Science, Aston University, Birmingham, UK

[2]School of Life and Health Sciences, Aston University, Birmingham, UK.

[3]Aston Research Centre for Healthy Ageing & School of Life and Health Sciences, Aston University, Birmingham, UK.

[4]Calon Cardio-Technology Ltd, Swansea, UK.

[5] School of Engineering, Griffith University, Gold Coast Campus, QLD 4222, Australia

Corresponding author details:

Dr Laura J Leslie,

Mechanical Engineering and Design,

Aston University,

Birmingham.

B4 7ET.

Fax number: 0044 (0)121 204 3676

Telephone number: 0044 (0)121 204 3747

Email address: l.j.leslie@aston.ac.uk and LJ_Leslie@hotmail.com

Running Title: Cell Exclusion in Couette Flow

Abstract

Introduction: Cell exclusion is the phenomenon whereby the haematocrit and viscosity of blood decreases in areas of high stress. Whilst this is well known in naturally occurring Poiseuille flow in the human body, it has never previously been shown in Couette flow, which occurs in implantable devices including blood pumps. The high shear stresses that occur in the gap between the boundaries in Couette flow is known to cause haemolysis in erythrocytes.

Materials and Methods: We propose to mitigate this damage by initiating cell exclusion through the use of a spiral groove bearing (SGB) which will provide escape routes by which the cells may separate themselves from the plasma and the high stresses in the gap. The force between two bearings (one being the spiral groove bearing) in Couette flow was measured. Stained erythrocytes, along with silver spheres of similar diameter to erythrocytes, were visualised across a transparent SGB at various gap heights.

Results: A reduction in the force across the bearing for human blood, compared to fluids of comparable viscosity, was found. This indicates a reduction in the viscosity of the fluid across the bearing due to a lowered haematocrit because of cell exclusion. The corresponding images clearly show both cells and spheres being excluded from the gap by entering the grooves. This is the first time the phenomenon of cell exclusion has been shown in Couette flow. It not only furthers our understanding of how blood responds to different flows but could also lead to improvements in the future design of medical devices.

Key Words: Erythrocytes, Hemolysis, Hemorrheology, Packed Red-Cell Volume, Ventricle-Assist Device

Introduction

Cell exclusion is the phenomenon that allows the viscous fluid that is blood, to travel through the narrow tubes of the body (i.e. the capillaries), under the force and pressure provided by the heart. Cells effectively 'thin out' as the blood is pumped through the narrow vessels, lowering the haematocrit and so the viscosity of the blood and allowing it to be pumped through these narrow vessels by the heart (1). This reduction in haematocrit and consequent reduction in viscosity is termed cell exclusion.

Previous studies have shown the existence of cell exclusion in Poiseuille flow - pressure-driven flow between stationary surfaces (e.g. in a pipe or capillary). This was shown with work in the 1930s wherein the viscosity of blood in different size tubes was measured, showing a reduction in viscosity and haematocrit in the narrowest tubes (1). This development has led to further research in the way in which blood cells behave in tubular flow.

The behaviour of blood cells within whole blood has been investigated over the years in various settings including the variation of haematocrit through glass chambers (2) and around obstacles such as stenosis (3). In addition, techniques such as fluorescence and particle image velocimetry (PIV) have been developed to better visualise the flow of cells(4). Evidence of cell exclusion in a VentrAssist blood pump with pad bearings has also been suggested through reduction in blood viscosity (5). However, cell exclusion in Couette flow, the flow in a gap between one rotating and one stationary surface, has not been previously been shown.

Couette flow-based medical devices, including implantable rotary blood pumps, can have traumatic and/or haemolytic effects on blood cells passing through them(6, 7). In order to improve the design of such devices, it is important to test for and aim to reduce cell damage and have a greater understanding of the behaviour of blood and its components when in contact with these devices(8, 9). In the case of implantable rotary blood pumps, cell damage including haemolysis is believed to be due to the small gaps inside the pump producing high levels of shear stress in Couette flow. Shear stress is known to exert a haemolytic effect on human blood both through continuous(10-13) and cyclic(14) application. Accepted wisdom (or design practice) recommends that in order to limit haemolysis, the size of the gap within a blood pump through which the blood passes must be kept above a minimum, damage-inducing level resulting in limitations in the way the pumps are designed.

In order to overcome this limitation, cell exclusion, such as that which occurs naturally in Poiseuille flow, could potentially protect the cells in Couette flow through the reduction of haematocrit in the areas of high stress.

Here we demonstrate for the first time, cell exclusion in Couette flow through the novel use of a spiral groove bearing (SGB), wherein the bearing operates with a viscosity lower than that of whole blood and where cell exclusion will have a significant anti-traumatic quality.

A SGB has one surface with a recurring pattern of grooves that is designated by logarithmic spirals (see Figure 1 for a cross-sectional view of the bearings). When one of the two parts of such a bearing is rotated with respect to the other, the viscous fluid in which the bearing is immersed is pumped through the grooves. Depending upon the direction of rotation and groove pattern, the fluid may either be pumped towards or away from the axis of rotation.

The flow rate in the grooves is dictated by the flow area available to allow fluid (blood) to escape from the grooves: this might be almost zero (corresponding to the greatest bearing force production). Muijderman(15) noted that there is no exchange of fluid between that within the gap and that outside the gap when flow area is reduced so as to prevent flow in the grooves; this might bring a distinct advantage when using a SGB as a blood bearing, as without transverse flow no blood cells will enter the gap once the rotor is started and this will be protective of the red cells.

In 1966 Muijderman(15) published work on the theory and application of various types of SGBs. Since then, the technology has attracted relatively little attention, with the major focus of application being in hard disc drive (HDD) and other high-speed spindle applications(16).

However, in 2004 Kink and Reul first proposed the use of a SGB as a blood bearing in miniature blood pumps. They identified SGBs as special type of hydrodynamic bearing that shows excellent load capacity and friction coefficient as compared to other types of hydrodynamic thrust bearings(17).

The aim was to demonstrate cell exclusion in Couette flow through the novel design and testing of a SGB which reduces red cell count in areas of high shear stresses leaving only (or predominantly) plasma in the gap. Two approaches were taken: 1) Through the linear relationship between force and viscosity, and 2) Through the visualisation of blood cells and equivalent analogues in Couette flow.

Methods and Methods

Spiral Groove Bearing Design

The SGB was designed using Computer Aided Design (CAD) software and the theoretical performance of the SGB can be predicted using Equation 1(15). Table 1 identifies the variables in Equation 1. The numerical values for the variables are explained.

$$F = \frac{K_1 C_2}{2} \frac{\omega}{h_0^2} \frac{\left(\frac{(h_0/h_2)}{1+(h_0/h_2)}\right)^2 \cot(\alpha)\left(1-\left(\frac{(h_0/h_2)}{1+(h_0/h_2)}\right)\right)\left(1-\left(\frac{(h_0/h_2)}{1+(h_0/h_2)}\right)^3\right)}{\left(1+\left(\frac{(h_0/h_2)}{1+(h_0/h_2)}\right)^3\right)^2 + 4\left(\frac{(h_0/h_2)}{1+(h_0/h_2)}\right)^3 \cot(\alpha)^2} \quad (1)$$

Where

$$K_1 = 3\pi\eta R^4\left(1-(r_i/r_o)^4\right)$$

$$C_2 = \frac{e^{\frac{-2\pi}{k}\left(1-\frac{2\alpha}{\pi}\right)\tan(\alpha)\frac{2}{1+\gamma}\frac{1+\gamma H^3}{1+H^3}} - (r_i/r_o)^4 e^{\frac{2\pi}{k}\left(1-\frac{2\alpha}{\pi}\right)\tan(\alpha)\frac{2}{1+\gamma}\frac{1+\gamma H^3}{1+H^3}}}{1-(r_i/r_o)^4}$$

The load capacity, F, of the hydrodynamic bearing may be calculated from Equation 1 by selecting values for each of the parameters. The outer radius, r_0, of the impeller was set at r_0 = 22 mm. The larger the surface area of the bearing the greater the load capacity; it follows

that the inner radius should be as small as possible. However, load capacity is relatively unaffected by decreasing the inner radius much past r_i = 12 mm.

The load capacity is maximal at groove angles between 12-17°; so the groove angle, α, was set to 15°. For similar reasons, the number of grooves, k, has been set to 15 in order to optimise the bearing performance whilst maintaining a degree of simplicity with respect to manufacture.

The optimum value of the ridge width-to-groove width ratio, γ, varies very little from 1 for various groove geometries; this value was used which simplifies the expression for the correction factor, C_2.

The relationship between groove height, h_2, and film thickness, h_0, is a more complex one; the optimum ratio is h_0:h_2 = 0.35; for a set groove height h_2 = 200 µm, the corresponding film thickness h_0 = 70 µm – but in use this ratio cannot be maintained as the film thickness h_0 varies. The groove height, h_2, of the SGB can be seen visually in Figure 1. Film thickness is determined by the gap between the bearings i.e. a gap height of 25 µm, would result in a film thickness, h_0, of the same value as can be seen in Figure 2.

The Rig & Loop

A rig was designed and built which allowed fluid to be passed between the two faces of the bearing. The lower face remained stationary and incorporated the spiral grooves; two versions of this face were made using a CNC milling machine (Fanuc Robodrill α-T21iE, FANUC Ltd., Oshino-mura, Japan): one was transparent to allow visual access through it during flow visualisation experiments, the second was of the same shape but fabricated from

stainless steel and used in the force measurement experiments. The upper, flat, stainless steel face rotated at a set speed (Figure 2) driven by the spindle of a milling machine (DYNA MYTE 2400, Dugard Machine Tools Ltd., Hove, UK).

A chamber lid was located on the base of the rig by a Perspex tube and clamped down to the base of the chamber. The chamber was sealed around the spindle using a rotating shaft seal that was mounted in the chamber lid. The lid had an inlet which supplied the fluid to the chamber and an overflow to ensure that the chamber was completely filled. The base had an outlet which flowed into a reservoir. Solutions were either pumped through the entire system in a closed loop using a (Jostra) RotaFlow system (MAQUET, Cardiovascular LLC, Wayne, NJ, USA) or were contained wholly within the chamber as an isolated volume.

Blood collection & handling

Two sources of blood were used with University Ethical Committee approval. Where small volumes (less than 100 ml) were required, peripheral venous blood was collected from human volunteers using a 19 gauge needle and placed immediately into heparinised tubes (International Scientific Supplies Ltd., Bradford, UK) to prevent clotting. All blood samples were prepared immediately, stored at room temperature (21°C) and used within one hour of collection. Red blood cells were separated using centrifugation at 1,000 g (centrifugal force) for 10 minutes, washed three times in PBS (Fisher Scientific UK Ltd., Loughborough, UK), and re-suspended in PBS at the desired haematocrit level. Where large volumes (greater than 100 mL) were required, research red cells were bought from the NHS (NHS Blood and Transplant, Watford, UK). These cells were prepared in the same way as the volunteered blood in terms of washing and re-suspension.

Force measurements

Before the chamber was filled, the face of the spindle (upper face) and (lower, stainless steel) bearing surface were brought into contact so that the separation gap was set to h_0 = 0 μm when the load cell first registered a load and a simple electrical resistance measurement between the two metallic rig components measured at 0 ohms. With the chamber filled with fluid, the spindle was withdrawn to the required gap height and rotated at a speed of 2500 rev/min and the load capacity (bearing force) was measured by the load cell (DBBSM-200N, Applied Measurements Ltd., Aldermaston, UK) as a function of gap height. The stiffness of the load cell was sufficiently high such that any force produced by the bearing did not alter the film thickness through compression of the load cell. The temperature of the fluid was maintained at a constant temperature of 22°C throughout the entire rig.

Tests were carried out initially with aqueous glycerol solutions at various percentages (0 to 36 % v/v at 22°C) so as to mimic the possible variation in blood viscosity due to cell exclusion i.e. if cells migrated to the grooves, only plasma would be left in the gap, therefore reducing the haematocrit and viscosity of the fluid and so the force between the bearings. Viscosity measurements were carried out using an Automated Micro Viscometer (Anton Paar GmbH, Graz, Austria) at temperatures between 20 and 25°C, measuring the sample four times at each temperature and using an average for the final reading. The solutions and viscosities are shown in Table 2. The measured viscosity of whole blood was lower than the normal value of 3-4 mPa·s (18, 19) due to the plasma (viscosity of around 1.3 mPa·s (19)) being replaced with PBS (viscosity of 1 mPa·s). This, however, does not preclude the comparison of blood of known viscosity with analogue fluids of known viscosities.

Flow visualisation

For visualisation of the flow across the SGB, the bottom section of the rig was replaced with a hollow equivalent manufactured from aluminium (Figure 3) and the metallic SGB was replaced with one machined from acrylic. This acrylic SGB disc was inserted into the hollow rig and was secured using a rubber O-ring. A circular mirror with 45°optic holder (Thorlabs Ltd, Cambridgeshire, UK) allowed optical access through a port in the side of the hollow rig to the underside of the acrylic bearing disc; approximately one quarter of the entire SGB could be viewed in this way.

A Particle Image Velocimetry (PIV) system (Nd:YAG laser, Flowsense camera with Nikon lenses and Version 2.30 Dynamic Studio software, Dantec Dynamics, Bristol, UK) was used to perform flow visualisation. The PIV system is capable of capturing images at up to 15 Hz frequency, but the spindle rotated at 41.6 Hz (2500 rev/min) so laser firing and camera shutter were synchronised to every 3^{rd} or 4^{th} revolution of the spindle through a trigger generated by a rotary encoder (BHK 16.24K360-I2-5, Baumer UK Ltd., Swindon, UK). In this way scratches in the image appeared stationary (in the same place) allowing image processing to mostly remove them. Only one Nd:YAG laser, wavelength 532 nm, in the PIV system was fired for image capturing. The beam was formed in to a sheet of around 4 mm thickness using a cylindrical lens ensuring even illumination of the entire viewing area and gap (which had a maximum height of interest of a few hundred micrometres).

In some experiments, silver spheres of diameter 10 µm (Dantec Dynamics) were suspended in aqueous glycerol as a blood analogue and sent through the rig. These spheres were very easy to visualise and do not have the optical density challenges of red blood cells, but have similar dimensions (red blood cells are 10 µm diameter by 2 µm thick discoids).

In order for the RBCs to be effectively imaged using the PIV system, cells were stained using PKH26, a red fluorescent cell membrane labelling kit (Sigma-Aldrich, Poole, UK) with an excitation maximum of 551 nm and emission maximum of 567 nm. The volumes of cells required for the imaging experiments were washed thoroughly before being suspended in the supplied diluent at the manufacturer's recommended cell concentration; cells were then stained according to the manufacturer's instructions. In order to optimise the staining methodology, both the cell concentration and incubation time of the procedure were varied and the resulting stained cells analysed for fluorescence using a flow cytometer (Quanta SC, Beckman Coulter, High Wycombe, UK). The optimal staining procedure for red cells was to initially suspend cells in a concentration of $1x10^{7}$ cells/mL in diluent C and to incubate this cell suspension with an equal volume $4x10^{-6}$ µM PKH26 for exactly 3 minutes before stopping the reaction by the addition of 10% serum (PAA Laboratories Ltd., Yeovil, UK). The resultant population of stained cells showed over 90% of the recognised RBCs to be fluorescing. Increased cell:dye ratios resulted in reduced fluorescence staining, whilst longer incubation times did not increase the percentage of cells fluorescing but did increase debris, possibly due to increased cell death in the population.

In order to view the PKH26 stained cells with more clarity in the PIV system, a filter (Polished Filter Glass, H.V. Skan Ltd., Solihull, U.K.) was used which blocked all wavelengths below 540 nm, including the light from the laser source, and allowed through the fluorescent light from the cells.

With the fluid in the transparent rig, images were captured at gap heights 25, 50, 75 and 100 µm. At each gap height between 10 and 30 images were captured. The Dynamic Studio software (V 2.30, Dantec Dynamics) was used to assemble a mean of the images, thereby

identifying the common marks e.g. groove edges and permanent marks. This image mean was then subtracted from each individual image, resulting in an image showing only the uniquely moving pixels. These resultant images were then summed together to show the total addition of all images at that gap height without any of the static patterning (i.e. all the scratches were removed).

Results and Discussion

Force measurements

The bearing force generated on the load cell was measured for a range of aqueous glycerol solution strengths (and viscosities) over a range of bearing gap sizes; Figure 4 shows one example of this for a 25 μm gap. A line fit through the data shows a linear relationship between force and viscosity for those fluids.

Bearing force measurements obtained with blood, 25% (v/v) aqueous glycerol and PBS as the working fluid in gaps of increasing height are reported in Figure 5. The expectation is that, for a given gap, a higher bearing force will be generated by a fluid of higher viscosity; PBS and aqueous glycerol conform to expectations.

However, Figure 5 shows the human blood to produce a lower than expected bearing force (than for a fluid of equal Newtonian viscosity). The average force measured at 25 μm for human blood was 4.58 N to 2 d.p. (decimal points) whereas the line-fit equation of Figure 4 would predict a force of 5.32 N. The same line-fit equation indicates an apparent viscosity of the blood to be 2.36mPa·s; 19% lower than the viscosity measured in the viscometer. Our explanation for this is that cell exclusion is occurring, whereby RBCs are entering the grooves in the SGB and becoming more densely packed in these grooves, leaving behind a fluid in the gap of lower haematocrit and therefore lower viscosity - which will generate lower bearing force. This apparent reduction in viscosity of blood in blood-filled bearings has been noted in practice in the operation of rotary blood pumps(5).

Blood viscosity is known to alter with shear rate $(\dot{\gamma})$, with an increasing shear rate resulting in a decrease in viscosity in a non-linear relationship (20). This mechanism was not significant at the shear rates experienced by the blood in the small gaps of our experiment, as shear rates well exceeded $1000s^{-1}$, beyond which point viscosity has become asymptotic (i.e. invariant with shear rate) (21).

Flow visualisation

Flow visualisation experiments aim to confirm the reduction in haematocrit in the bearing gap indicated by the bearing force measurements reported above and to show that cells preferentially travel in the grooves rather than in the bearing gap for small bearing gaps.

Image Analysis

The images in Figure 6 show the image analysis sequence of the pictures captured at a 25μm gap height for silver spheres. This sequence allows common pixels which occur on every image, such as scratches, marks and groove outlines, to be subtracted from the final images. The addition of several images together allows an overview of what is occurring over time. The drawback to this analysis include the potential loss of data where, for example, moving spheres are occurring in every image at the same position due to the high density and so are subtracted as part of the mean. However, by comparing the raw image with the same image minus the mean, it is clear that a much more useful image is obtained, without background interference.

Red Blood Cells

Red blood cells stained with PKH26 were observed in the transparent SGB and the images analysed per the sequence described. The images from the RBCs were not as readily acquired

as for the silver spheres, with the optical density of the cells blocking the laser light at high haematocrits. To give an indication of the movement of the cells, a haematocrit of less than 1% was used. Results from this experiment are shown in Figure 7. The RBCs are difficult to image due to limited fluorescence and the optical density of the filter but a pattern of bright spots (striations) representing cells bounded by the grooves can be seen in Figure 7 (a) at a gap height 25 µm. This pattern appears less obvious in Figure 7 (b) and Figure 7 (c) as the gap height increases (to 50 and 75 µm respectively) and when the gap height reaches 100 µm in Figure 7 (d), the cells appear to be completely randomly spread (moving readily in the gap and grooves), suggesting that cell exclusion is no longer occurring at the same intensity as in the smaller gaps.

Silver Spheres

The silver spheres were more readily imaged in comparison to the stained RBCs and so were used to identify areas of 'cell' population density. Figure 8 shows analysed images for gap heights 25, 50, 75 and 100 µm. Figure 8 (a) shows cell exclusion occurring at a 25 µm gap height, with almost no spheres outside of the grooves and in the gap. At a 50 µm gap height (Figure 8 (b)), some spheres are visible. At 75 µm (Figure 8 (c)) more spheres again are in the gap and at 100 µm (Figure 8 (d)) there are even more spheres in the gap, outside of the grooves.

Conclusions

Spiral groove bearings find wide applications in engineered products such as in the air bearings of hard disk drives for computers (16), but particle exclusion and viscosity changes (other than due to temperature) are not significant effects where Newtonian fluids are used. For blood, a non-Newtonian fluid, the SGB has shown a very interesting effect.

Bearing force measurements indicate a reduction in viscosity of blood in small Couette gaps and it is proposed here that this reduction in viscosity is a result of red blood cells being excluded from the working portion of the bearing – i.e. the gap between bearing faces. The relationship between blood viscosity and haematocrit is well known and has been studied under many different conditions(19).

Flow visualisation of red blood cells traversing a spiral groove bearing shows cell exclusion of the red cells from the narrowest of gaps (25 μm) with a propensity for the red cells to remain in the deeper grooves. This cell-exclusion effect weakens with increasing gap height. Suspended solutions of silver spheres of similar dimensions to red blood cells (10 μm diameter) show the same trend, but are much easier to visualise as they reflect incident light much better due to their coating.

Cell exclusion in small capillary tube (Poiseuille) flow is also well known since the pioneering work of Fåhraeus and Lindqvist in the 1930's. This paper demonstrates that cell exclusion mechanisms also work in small Couette gaps when alternative flow paths for red blood cells are provided – the example here is spiral grooves.

This finding has two major implications for the design of a number of medical devices – most notably rotary blood pumps:

1. Restoring forces developed by blood-filled bearings (which invariably incorporate small gaps) will be lower than calculated using Muijderman's spiral groove bearing equations (and, by suggestion using Reynolds equation for journal bearing equations).
2. Small gaps can be protective of red blood cells. This is counterintuitive and contrary to popular design codes for rotary blood pumps which seek to maximise the gap and thus protect red blood cells through reducing the shear stress developed in the blood.

The next stage in this research is to quantify the protective effect of cell exclusion in Couette flow. We propose to do this through the measurement of haemolysis levels and pro-thrombotic PS exposure of the red cells, and the inflammatory response of white cells in Couette flow, with and without a spiral groove bearing.

Acknowledgements

The authors would like to thank the technical staff in Mechanical Engineering and Design at Aston University for their assistance in this project. They would also like to thank NHS Blood & Transplant for their permission to use their products for this research.

References

1. Fåhraus R, Lindqvist T. THE VISCOSITY OF THE BLOOD IN NARROW CAPILLARY TUBES. *Am J Physiol*. 1931;96(3):562-8.

2. Palmer AA. Axial drift of cells and partial plasma skimming in blood flowing through glass slits. *American Journal of Physiology -- Legacy Content*. 1965;209(6):1115-22.
3. Fujiwara H, Ishikawa T, Lima R, Matsuki N, Imai Y, Kaji H, et al. Red blood cell motions in high-hematocrit blood flowing through a stenosed microchannel. *Journal of Biomechanics*. 2009;42(7):838-43.
4. Sugii Y, Okuda R, Okamoto K, Madarame H. Velocity measurement of both red blood cells and plasma of in vitro blood flow using high-speed micro PIV technique. *Measurement Science and Technology*. 2005;16(5):1126.
5. Vidakovic S, Ayre P, Woodard J, Lingard N, Tansley G, Reizes J. Paradoxical Effects of Viscosity on the VentrAssist Rotary Blood Pump. *Artificial Organs*. 2000;24(6):478-82.
6. Sutera S. Flow-induced trauma to blood cells. *Circ Res*. 1977;41(1):2-8.
7. Kawahito K, Nose Y. Hemolysis in different centrifugal pumps. *Artif Organs*. 1997;21(4):323-6.
8. Patrick M, Chen C-Y, Frakes D, Dur O, Pekkan K. Cellular-level near-wall unsteadiness of high-hematocrit erythrocyte flow using confocal µPIV. *Experiments in Fluids*. 2011;50(4):887-904.
9. James NL, Wilkinson CM, Lingard NL, Meer ALvd, Woodard JC. Evaluation of Hemolysis in the VentrAssist Implantable Rotary Blood Pump. *Artificial Organs*. 2003;27(1):108-13.
10. Watanabe N, Arakawa Y, Sou A, Kataoka H, Ohuchi K, Fujimoto T, et al. Deformability of human red blood cells exposed to a uniform shear stress as measured by a cyclically reversing shear flow generator. *Physiol Meas*. 2007;28(5):531-45.
11. Nanjappa BN, Chang H-K, Glomski CA. Trauma of the Erythrocyte Membrane Associated with Low Shear Stress. *Biophysical Journal*. 1973;13(11):1212-22.
12. Leverett LB, Hellums JD, Alfrey CP, Lynch EC. Red blood cell damage by shear stress. *Biophys J*. 1972;12(3):257-73.
13. Paul R, Apel J, Klaus S, Schügner F, Schwindke P, Reul H. Shear Stress Related Blood Damage in Laminar Couette Flow. *Artificial Organs*. 2003;27(6):517-29.
14. Lee SS, Antaki JF, Kameneva MV, Dobbe JG, Hardeman MR, Ahn KH, et al. Strain Hardening of Red Blood Cells by Accumulated Cyclic Supraphysiological Stress. *Artificial Organs*. 2007;31(1):80-6.
15. Muijderman EA. Spiral groove bearings library Pt, editor. New York: Springer-Verlag; 1966. 199 p.
16. Zou Q, Tian Y, Liu X, Wen S, Barber GC. Study of Flow Characteristics of Lubricant in Spiral-Groove Bearings by the Fluorescent Method. *Tribology Transactions*. 2005;48(2):259 - 63.
17. Kink T, Reul H. Concept for a new hydrodynamic blood bearing for miniature blood pumps. *Artificial Organs*. 2004;28(10):916-20.
18. Lowe G, Fowkes F, Dawes J, Donnan P, Lennie S, Housley E. Blood viscosity, fibrinogen, and activation of coagulation and leukocytes in peripheral arterial disease and the normal population in the Edinburgh Artery Study. *Circulation*. 1993;87(6):1915-20.
19. Wells RE, Jr., Merrill EW. Influence of flow properties of blood upon viscosity-hematocrit relationships. *J Clin Invest*. 1962;41:1591-8.
20. Wells RE, Merrill EW. Shear Rate Dependence of the Viscosity of Whole Blood and Plasma. *Science*. 1961;133(3455):763-4.
21. Chien S. Shear Dependence of Effective Cell Volume as a Determinant of Blood Viscosity. *Science*. 1970;168(3934):977-9.

FIGURE LEGENDS

Figure 1 Cross-section of the SGB design in the experimental setting showing groove height h_2 and gap height (or film thickness) h_0

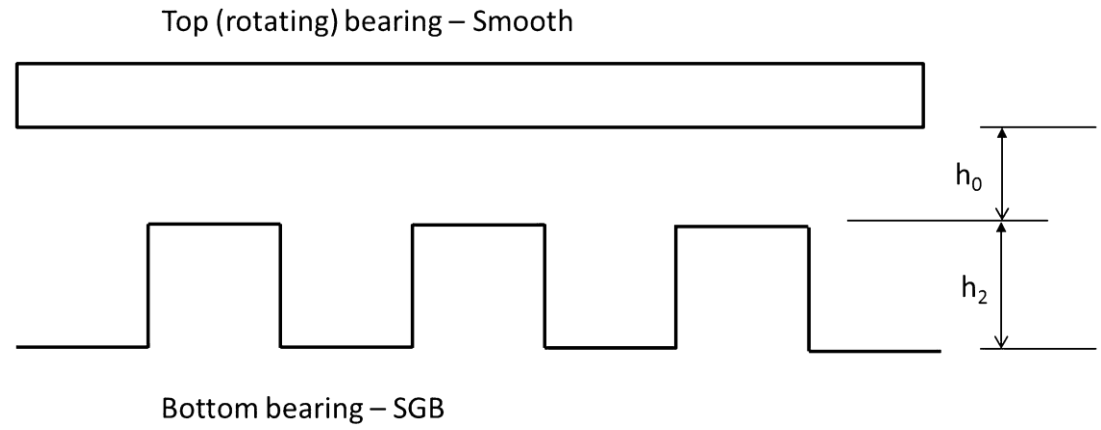

Figure 2: The rig containing the SGB through which the fluid was pumped

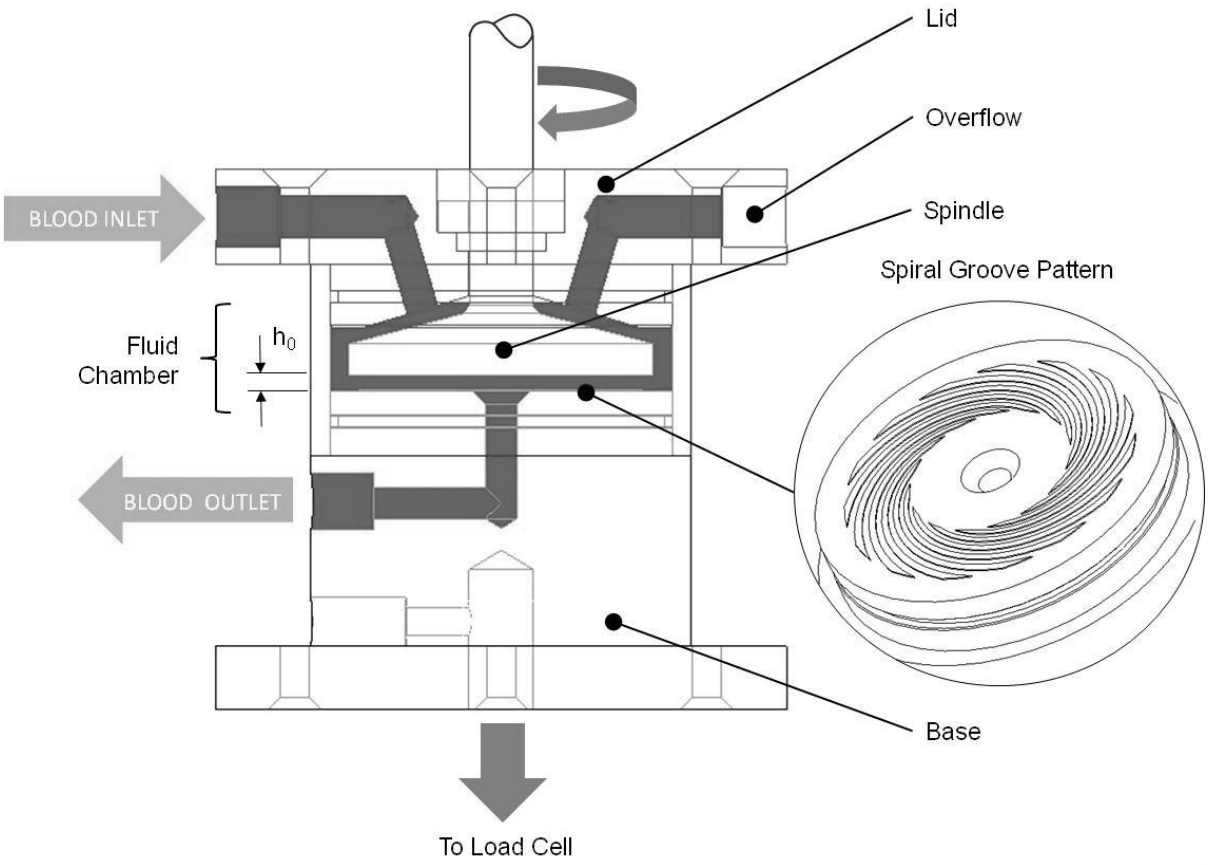

Figure 3: Hollow rig allowing optical access to the lower spiral-grooved disc

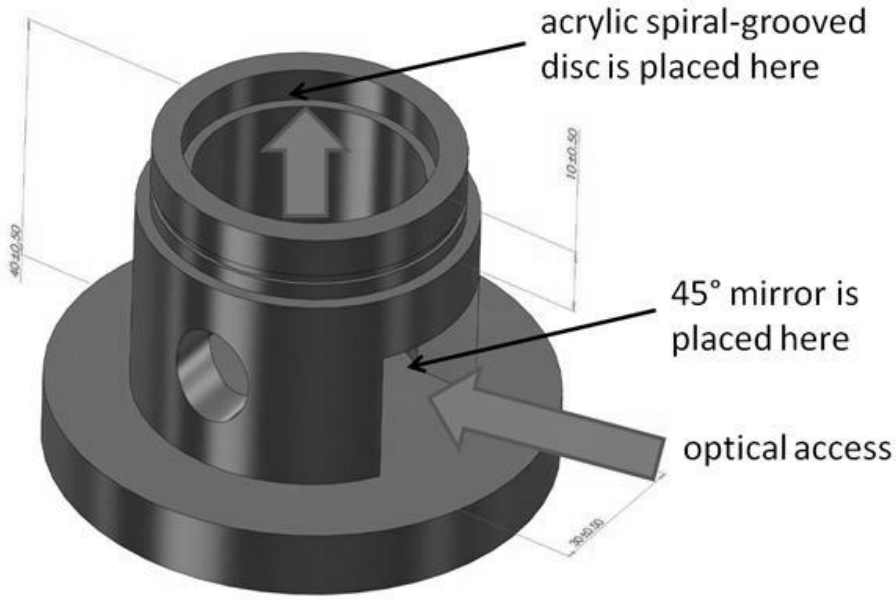

Figure 4: Force vs. viscosity at a 25 µm gap height and 2500 rev/min rig speed for aqueous glycerol and the three blood samples. For the aqueous glycerol solutions, the linear line fit gives $y=1.63x+0.74$, $R^2=0.99$ (to 2d.p.)

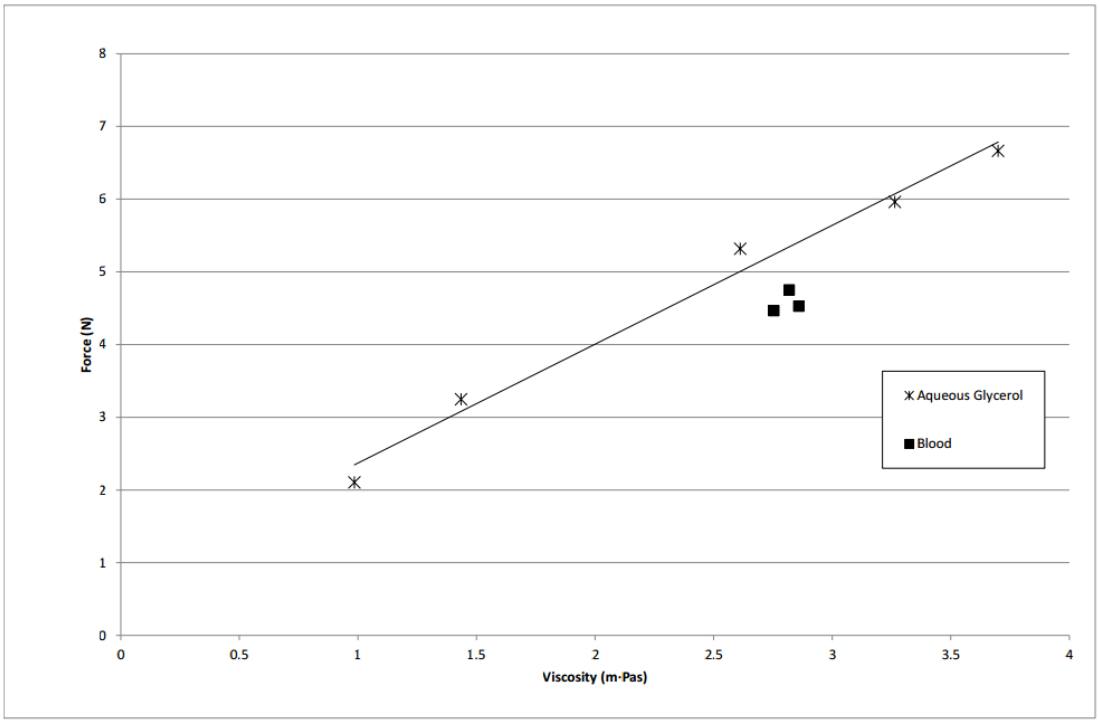

Figure 5: Force Vs. gap height measurements for different fluids at rig speed 2500 rev/min

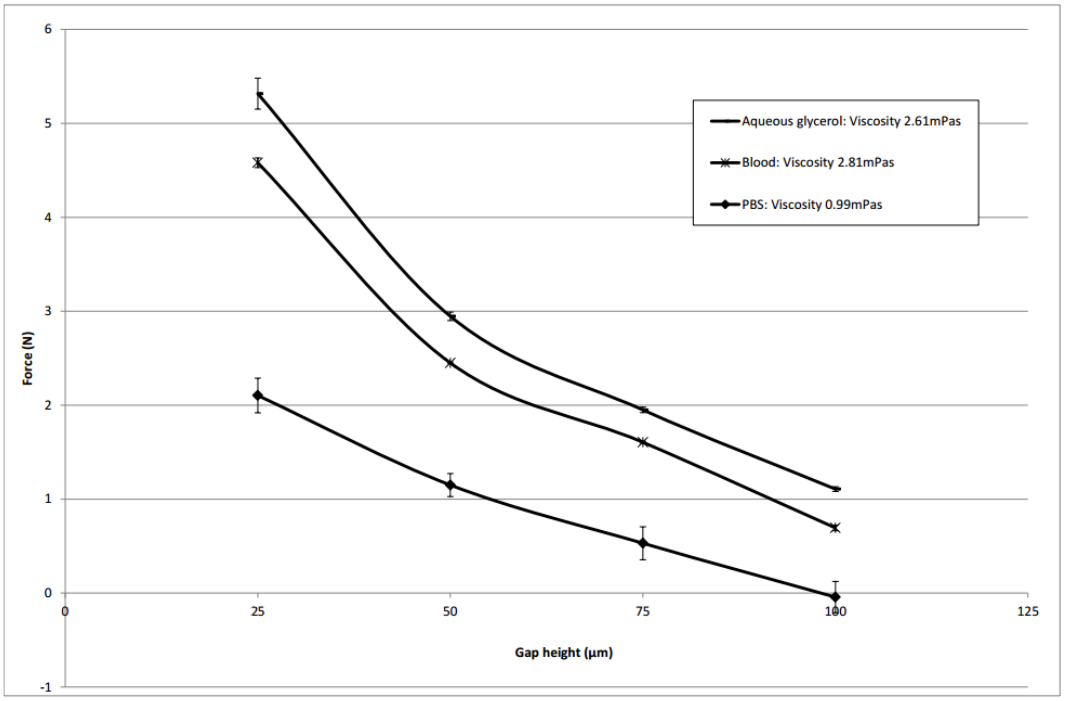

Figure 6: Image analysis of silver spheres in a 25 µm gap height. (a) The raw image, (b) the mean image from 10 raw images, (c) one raw image with the mean subtracted and (d) the addition of 10 images (after individual mean subtraction).

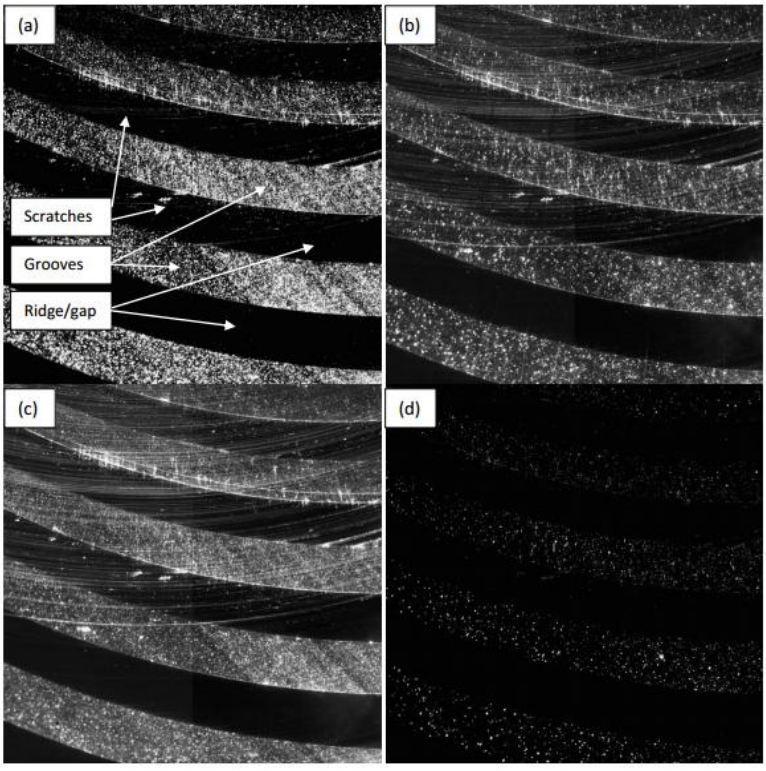

Figure 7: Analysed images of RBCs at gap heights (a) 25 µm (b) 50 µm (c) 75 µm and (d) 100 µm. At gap height 25 µm, a small number of fluorescing cells can be seen in the grooves, with no bright pixels in the gap. As the gap size increases, the number and intensity of the bright pixels, fluorescing cells, increases, indicating the cells leaving the grooves and entering the gap as cell exclusion becomes less apparent.

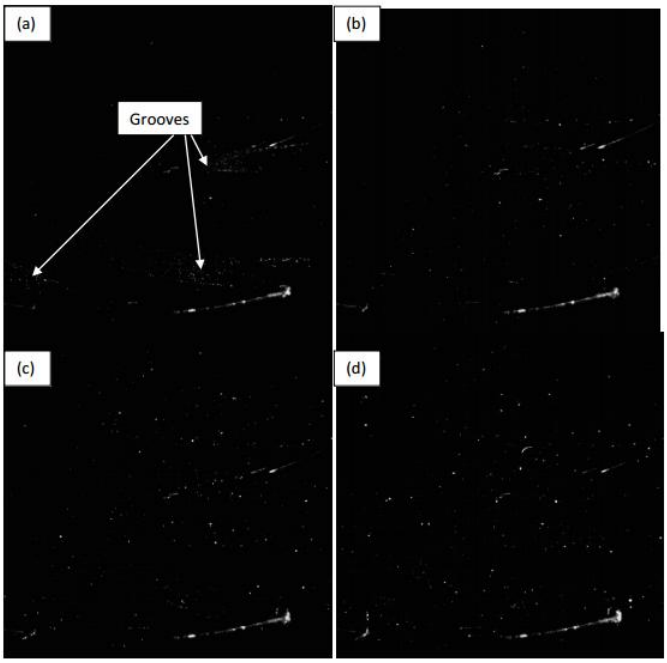

Figure 8: Analysed images of silver spheres at gap heights (a) 25 µm (b) 50 µm (c) 75 µm and (d) 100 µm.

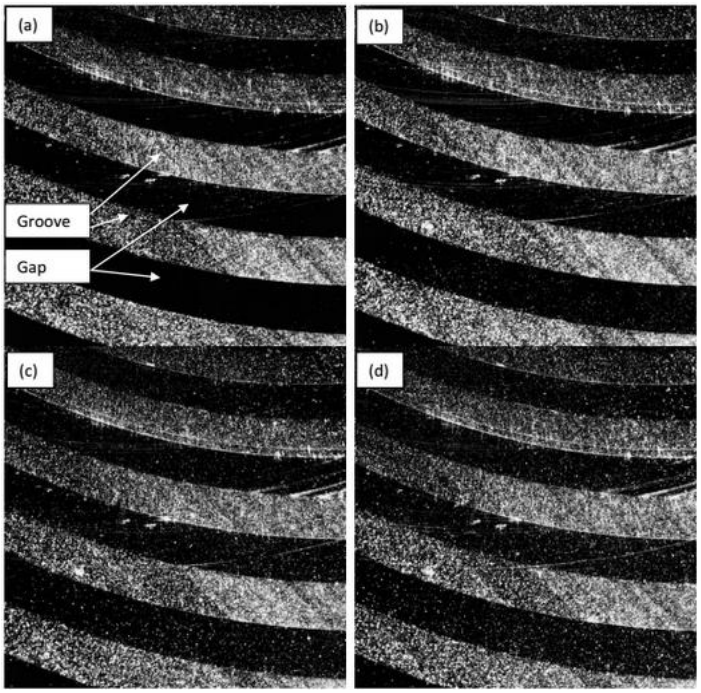

TABLES

Table 1: Spiral groove parameters

Parameter	**Symbol**
Load capacity (N)	F
Outer radius (m) (= 0.022 m)	$R = r_0$
Inner radius (m) (= 0.012 m)	r_i
Groove angle (degrees) (= 15°)	α
Film thickness (m) (70 μm at optimum conditions)	h_0
Groove height (m) (=200 μm)	h_2
Angular velocity (radians/s) (= 210 radians/s)	ω
r_i / r_o (= 0.7727)	λ
Ridge width-to-groove width ratio (= 1)	γ
Viscosity (mPa·s) (=0.99 to 3.70mPa·s)	η

Table 2: Measured viscosities of analogous solutions at 22°C

Fluid	**Measured dynamic viscosity μ (mPa·s) to 2 d.p.**
Phosphate buffered solution (PBS)	0.99
Aqueous glycerol A	1.44
Aqueous glycerol B	2.61
Aqueous glycerol C	3.27
Aqueous glycerol D	3.70
Human blood (~45% haematocrit in PBS)	2.81